Medical Engineering and Physics 49 (2017) 46–55

Contents lists available at ScienceDirect

Medical Engineering and Physics

journal homepage: www.elsevier.com/locate/medengphy

The variation in frequency locations in Doppler ultrasound spectra for maximum blood flow velocities in narrowed vessels

Yingyun Zhang[a], Yufeng Zhang[a,*], Lian Gao[a], Li Deng[a], Xiao Hu[a], Kexin Zhang[b], Haiyan Li[a]

[a] Department of Electronic Engineering, Information School, Yunnan University, Kunming, Yunnan 650091, China
[b] The Second Affiliated Hospital of Kunming Medical University, Kunming, Yunnan 650031, China

ARTICLE INFO

Article history:
Received 16 February 2017
Revised 8 July 2017
Accepted 14 July 2017

Keywords:
Doppler ultrasound
Maximum blood flow velocity
Stenosed vessel
Doppler frequency shift

ABSTRACT

This study assessed the variation in the frequency locations in the Doppler ultrasound spectra for the maximum blood flow velocities of in vessels with different degrees of bilaterally axisymmetric stenosis. This was done by comparing the relationship between the velocity distributions and corresponding Doppler power spectra. First, a geometric vessel model with axisymmetric stenosis was established. This made it possible to obtain the blood flow velocity distributions for different degrees of stenosis from the solutions of the Navier–Stokes equations. Then, the Doppler spectra were calculated for the entire segment of the vessel that was covered by the sound field. Finally, the maximum frequency locations for the spectra were determined based on the intersections of the maximum values chosen from the calculated blood flow velocity distributions and their corresponding spectra. The computational analysis showed that the maximum frequencies, which corresponded to the maximum blood flow velocities for different degrees of stenosis, were located at different positions along the spectral falling edges. The location for a normal (stenosis free) vessel was in the middle of the falling edge. For vessels with increasing degrees of stenosis, this location shifted approximately linearly downward along the falling edge. For 40% stenosis, the location reached a position at the falling edge of 0.32. Results obtained using the Field II simulation tool demonstrated the validity of the theoretical analysis and calculations, and may help to improve the maximum velocity estimation accuracy for Doppler blood flow spectra in stenosed vessels.

1. Introduction

The variation in the maximum blood flow velocity, which corresponds to the maximum frequency shift in the results of a Doppler ultrasound test, can reflect the blood flow conditions of vessels [1]. Accordingly, several parameters are used to diagnose cardiac and cerebrovascular diseases (atherosclerosis, stroke, etc.). These parameters include the systole and diastole (S/D) velocity ratio, resistance index (RI), and pulsatility index (PI) [2,3]. It is significant to accurately estimate the maximum blood flow velocity in vessels, especially for those with different degrees of stenosis.

Clinics and studies commonly use the Doppler blood flow spectrum to determine the maximum frequency. Then the maximum blood flow velocity is calculated using the Doppler equation [4]. Commonly used algorithms include the simple threshold method (STM) [5], percentile method (PM) [6], threshold-crossing method (TCM) [7], modified threshold-crossing method (MTCM) [5,8], and hybrid method (HM) [7]. The STM employs a user-determined threshold to yield the maximum frequency envelope superimposed on a sonogram. The PM calculates the total power for each spectral estimate, and then determines the frequency below which a given percentage of the total power lies. These values are typically 75–95% of the total power. The TCM and MTCM are based on the assumption that the noise superimposed on a signal can be modeled as a white Gaussian process, i.e., with a constant spectral density over the analyzed bandwidth. The tail of the Doppler spectrum is used to determine that noise level. The HM combines features of both the PM and TCM. Although the abovementioned methods are simple and easy to implement, because of the intrinsic spectral broadening [9] and estimated spectral window broadening [10,11], it is difficult to objectively and accurately confirm the maximum frequency of a Doppler blood flow spectrum. Moreover, in practice, Doppler blood flow signals are inherently subject to interference by extraneous noise, and depending on their source and magnitude, the actual Doppler spectra may to some extent be contaminated. In this case, the reliability could be limited for maximum blood flow velocities estimated using the maximum frequencies extracted from polluted spectra [12].

In order to overcome the deficiency of these traditional methods, Vilkomerson et al. proposed a novel approach for using the Doppler spectrum of a normal (stenosis-free) blood vessel to deter-

* Corresponding author.
E-mail addresses: yfengzhang@yahoo.com, zhangyf@ynu.edu.cn (Y. Zhang).

http://dx.doi.org/10.1016/j.medengphy.2017.07.004
1350-4533/

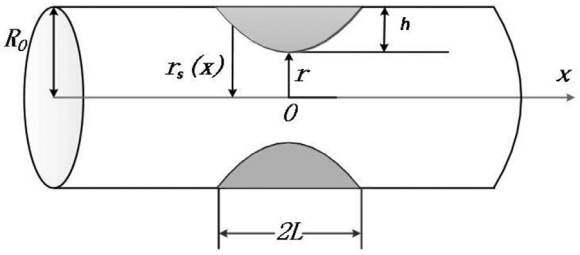

Fig. 1. Geometric vessel model of bisymmetric stenosis.

mine its maximum blood flow velocity [13]. The main idea in that approach was that the theoretical Doppler blood flow spectrum was calculated based on the parabolic velocity distribution of a normal vessel. Then, corresponding maximum frequency locations for the spectrum were determined based on the intersection of the theoretical maximum velocity and calculated spectrum. Finally, the maximum blood flow velocity was calculated according to the Doppler equation. The results showed that for a normal vessel, the maximum frequency location is the middle of the falling edge. Additionally, the noise pollution in the spectrum could be offset in the calculation process, because the position at the spectral falling edge was confirmed by a subtraction operation between the maximum and minimum power values. Therefore, noise interference was effectively avoided. The validity and reliability of this approach were higher than those of traditional methods [13]. However, this research involved a normal vessel, in which blood flow is assumed to have a parabolic distribution under steady flow conditions. In clinical practice, diseased vessels may be narrowed, which leads to a more complicated blood flow status, with broader spectra compared to those for normal vessels. As a result, the previously mentioned results for a normal vessel are not applicable. Thus, it is necessary to investigate the variation between the maximum blood flow velocities and Doppler spectra frequency locations in stenotic vessels.

In this study, we investigated the relationship between the blood flow velocity and the Doppler power spectrum for a stenosed vessel, in order to obtain the variation between the maximum velocities and spectrum frequency locations for vessels with different degrees of bilaterally axisymmetric stenosis. First, a geometric vessel-model with axisymmetric stenosis was established to obtain the analytic form of the flow velocity distributions for different degrees of stenosis according to the Navier–Stokes equation (NSE). Because of the approximately constant velocity in each shell along the vessel segment of the sample volume, the spectrum model proposed by Vilkomerson et al. [13] was used to calculate the blood flow spectra by moving the particles according to the obtained velocity distribution at the narrowest position. During the observation time interval, the power spectrum of the windowed signal for each particle was the square of the line spectrum, whose frequency corresponded to the moving velocity. This value was multiplied by the *Sinc* function, and the values were accumulated to yield the Doppler spectra for the entire segment of the vessel covered by the sound field. Finally, the corresponding maximum frequency locations for the spectra were determined based on the intersections of the maximum values chosen from the blood flow velocity distributions and their calculated spectra. In the theoretical calculations, the locations of normal vessels and those with 5%, 10%, 20%, 30%, and 40% stenosis were separately confirmed. Then, the variation between the maximum velocities and their frequency locations in the spectra of the vessels with different degrees of stenosis was acquired. In order to verify the theoretical analysis and computation results, a simulation assessment based on the Field II software platform was performed. A dynamic scatterer phantom for vessels with different degrees of stenosis was established to simulate the Doppler ultrasound blood flow signals in Field II. The corresponding spectra were calculated using a short time Fourier transform (STFT), and the locations of the maximum frequencies on the STFT-based spectra were confirmed. For validation, the simulation results were compared to those from the theoretical calculations.

2. Theoretical calculation based on spectral model

2.1. Stenosed vessel model

A cosine-formed vessel portion with axially symmetric stenosis is assumed to be established as a rigid tube with a circular cross section. Let x axis be the axis of the vessel, while r indicates the radial coordinates. The geometry of the stenosis is shown in Fig. 1 and described as follows:

$$r_s(x) = R_0\left[1 - \frac{h}{2R_0}\left(1 + \cos\frac{\pi x}{L}\right)\right],\ x \in [-L, L], \tag{1}$$

where $r_s(x)$ denotes the radius of the cosine-shaped vessel segment in the constricted region, R_0 is the constant radius of the straight artery in the non-stenotic segment, $2L$ is the axial length of the stenosis, and $h/R_0\%$ is the measurement of the degree of stenosis.

2.2. Blood flow velocity distributions

The blood in the axisymmetric stenotic-segment is assumed to be an incompressible Newtonian fluid. Since the axial velocity V_a and radial velocity V_r satisfy the NSEs [14,15], it follows that:

$$\begin{aligned}
&\frac{\partial V_a}{\partial x} + \frac{1}{r}\frac{\partial (rV_r)}{\partial r} = 0\\
&\frac{\partial V_a}{\partial t} = -\frac{1}{\rho}\frac{\partial p}{\partial x} + \frac{\alpha}{\rho}\left(\frac{\partial^2 V_a}{\partial r^2} + \frac{1}{r}\frac{\partial V_a}{\partial r}\right)\\
&\frac{\partial p}{\partial r} = \frac{\partial p}{\partial \varphi} = 0,
\end{aligned} \tag{2}$$

where p is the pressure, ρ is the blood density, α is the dynamic viscosity of the blood, and t is the time.

The vessel is assumed to be a straight rigid-tube, and the blood flow along the vessel walls cannot slip. Then, the velocity boundary conditions [16] along the vessel wall are taken as follows:

$$V_r|_{r=r_s} = 0; \quad V_a|_{r=r_s} = 0. \tag{3}$$

At the same time, the velocity condition of the symmetry axis is described as follows:

$$\left.\frac{\partial V_a}{\partial r}\right|_{r=0} = 0. \tag{4}$$

In order to solve the velocity distributions, the relevant flow parameters, such as pressure gradient $\frac{\partial p}{\partial x}$, axial velocity V_a, and radial velocity V_r can be expressed using the Fourier series in the following complex exponential:

$$\begin{aligned}
\frac{\partial p}{\partial x} &= C_0 + Re\left(\sum_{j=1}^{N} C_j e^{i\omega_j t}\right)\\
V_a &= V_{a0} + Re\left(\sum_{j=1}^{N} V_{aj} e^{i\omega_j t}\right)\\
V_r &= V_{r0} + Re\left(\sum_{j=1}^{N} V_{rj} e^{i\omega_j t}\right),
\end{aligned} \tag{5}$$

where $\omega_j = j\omega = j\frac{2\pi}{T}$ represents the angular frequency, T denotes the cardiac cycle, $Re(\cdot)$ is a function used to obtain the real component of a complex number, and $i = \sqrt{-1}$. In the Fourier series

expansion, $N=14$ can produce a suitable approximation of the human body physiology parameters [17].

It is assumed that the pressure gradient (C_0 and C_j) is known. By substituting (5) into (2) and using boundary conditions (3) and (4), the following axial and radial velocity distributions of the pulsatile blood flow in the vessels with various degrees of stenosis (y) are obtained [18,19]:

$$V_a(y,t) = \frac{{r_s}^2}{4\alpha}\left(y^2 - {y_1}^2\right)C_0 + Re\left(\sum_{j=1}^{N}\frac{{r_s}^2}{i\alpha\beta_j^2}\left[\frac{J_0\left(i^{3/2}\beta_j y\right)}{J_0\left(i^{3/2}\beta_j y_1\right)} - 1\right]C_j e^{i\omega_j t}\right) \tag{6}$$

$$V_r = \frac{{r_s}^2 y}{14\alpha}\left[4y_1 y_1' C_0 + \left(2y_1^2 - y^2\right)\frac{dC_0}{dx}\right] + \mathrm{Re}\left(\sum_{j=1}^{N} -\frac{{r_s}^3}{i\alpha\beta_j^2}\left[\begin{array}{l}\left(\frac{1}{i^{3/2}\beta_j}\frac{J_0\left(i^{3/2}\beta_j y\right)}{J_0\left(i^{3/2}\beta_j y_1\right)} - \frac{y}{2}\right)\frac{dC_j}{dx} \\ +\frac{J_1\left(i^{3/2}\beta_j y_1\right)J_1\left(i^{3/2}\beta_j y\right)}{{J_0}^2\left(i^{3/2}\beta_j y_1\right)}y_1' C_j\end{array}\right]e^{i\omega_j t}\right), \tag{7}$$

where $y = \frac{r}{R_0}$, $y_1 = \frac{r_s(x)}{R_0}$, $\beta_j = R_0\sqrt{\frac{\rho\omega_j}{\alpha}}$, $y_1' = \frac{dy_1(x)}{dx}$, and J_0 and J_1 are Bessel functions of the first kind of orders zero and one, respectively.

In order to acquire the pressure gradient coefficients (C_0 and C_j), the centerline velocity V_a^* for the upstream stenotic arterial segment at a certain position without stenosis is obtained using the ultrasound Doppler technique. Its Fourier series expansion is written as follows:

$$V_a^* = V_{a0}^* + Re\left(\sum_{j=1}^{N} V_{aj}^* e^{i\omega_j t}\right). \tag{8}$$

By substituting boundary condition (3) into radial velocity distribution (7) to yield a differential equation of the pressure gradient coefficients (C_0 and C_j), which is then solved using the boundary condition obtained from Eq. (8), the following coefficients are obtained [20]:

$$C_0 = -\frac{4\alpha V_{a0}^*}{R_0^2}\frac{1}{y_1^4} \tag{9}$$

$$C_j = i\alpha\beta_j^2 V_{aj}^* \Big/ \left\{R_0^2\left[\frac{1}{J_0\left(i^{3/2}\beta_j\right)} - 1\right]\right\} \times \frac{J_0\left(i^{\frac{3}{2}}\beta_j\right)}{\left(i^{\frac{3}{2}}\beta_j\right)^2 J_0\left(i^{\frac{3}{2}}\beta_j\right) - 2i^{\frac{3}{2}}\beta_j J_0\left(i^{\frac{3}{2}}\beta_j\right)} \times \frac{J_0(y_2)}{y_2^2 J_0(y_2) - 2y_2 J_1(y_2)}. \tag{10}$$

Finally, the axial and radial velocity distributions of the blood flow in a stenotic vessel are obtained by substituting C_0 and C_j into Eqs. (6) and (7), respectively. The following parameters are used to calculate the velocity distributions: the constant radius of the straight artery in the non-stenotic region $R_0 = 5$ mm, the stenotic length of vessel $2L = 8R_0 = 40$ mm, blood viscosity $\alpha = 3.5\times10^{-3}$ Pa s, and blood density $\rho = 1050\,\mathrm{kg/m^3}$. The centerline velocity waveform in the upstream stenotic arterial segment at some position (detected using a portable Doppler ultrasound device) is shown in Fig. 2 [21]. Figs. 3 and 4 show the axial and radial velocity distributions for vessels with various degrees of stenosis (0% (i.e., normal), 5%, 10%, 20%, 30%, and 40%) at different axial positions ranging from −10 to 10 mm at the time of the systolic peak (0.2 s). We can observe from Fig. 3 that for a normal vessel (Fig. 3(a)), the axial velocity distributions are parabolic in the radial direction, without any change along the axial direction. However, the velocities reach their maximum values at the most stenotic axial positions in stenosed vessels, and decrease with increasing axial distance (decrease in stenosis degree) until the end of the stenosis. Moreover, in the vessels with various degrees of stenosis, the maximum velocities at the most stenotic positions obviously increase with increasing stenosis. Compared with those in normal vessels, the velocity distributions in the radial direction do not maintain parabolic characteristics. This result indicates that the Doppler spectrum for the blood flow in a stenotic vessel may be different than that for parabolic blood flow. Therefore, the locations of the maximum velocities of the Doppler blood flow spectra for stenotic vessels could also be different from the maximum velocity locations for normal vessels. Axially antisymmetrical velocity profiles of the radial blood flow in vessels with stenosis are presented in Fig. 4(b)–(f). It should be noted that the radial velocities are significantly smaller than the axial velocities (Fig. 3), and their contributions to the Doppler spectra are therefore omitted here.

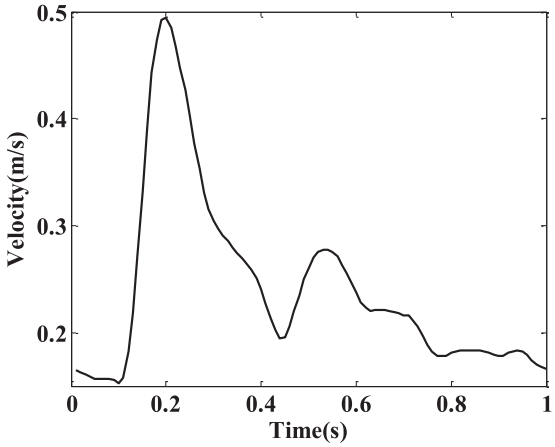

Fig. 2. Axial centerline velocity waveform of upstream segment in vessel.

2.3. Calculation of Doppler blood flow spectrum

Blood flow is assumed to travel through a stenotic vessel of diameter $2R_0$ insonated by a transducer (that is transmitting transducer, TX) producing a continuous ultrasound beam of wavelength λ. A second transducer (also called a receiving transducer, RX) at an angle of φ to the flow direction receives the Doppler ultrasound echoes from all of the moving scatterers. The transducers are arranged so that all of the flow components traveling through the cylindrical tube region of length D are insonated, and the backscattered signals generated from all of the flow components are received. The insonated model is shown in Fig. 5.

W uniformly distributed scatterers mimic the ultrasound scattering material (such as red blood cells) in a vessel with length $4L$. A Doppler shift can be formed from the movement of the scatterers with the movement of the blood. As shown in Fig. 3, the axial velocities for the same radial position but different axial locations along the longitudinal vessel are actually not constant. However, for a relative small observed segment (centered at the location of the narrowest lumen), the changes in these axial velocities are small. For example, in the vessel with 40% stenosis (the highest degree of stenosis) shown in Fig. 3(f), the maximum relative peak velocity differences (at a radial position of 0 mm) for observational widths of 2 mm, 4 mm, and 6 mm are 0.43%, 0.91%, and 2.10%, respectively. For this reason, the velocity in each shell throughout an observational segment of the stenosed vessel can be considered to be approximately constant. Thus, the spectrum model proposed by Vilkomerson et al. [13] is used to calculate

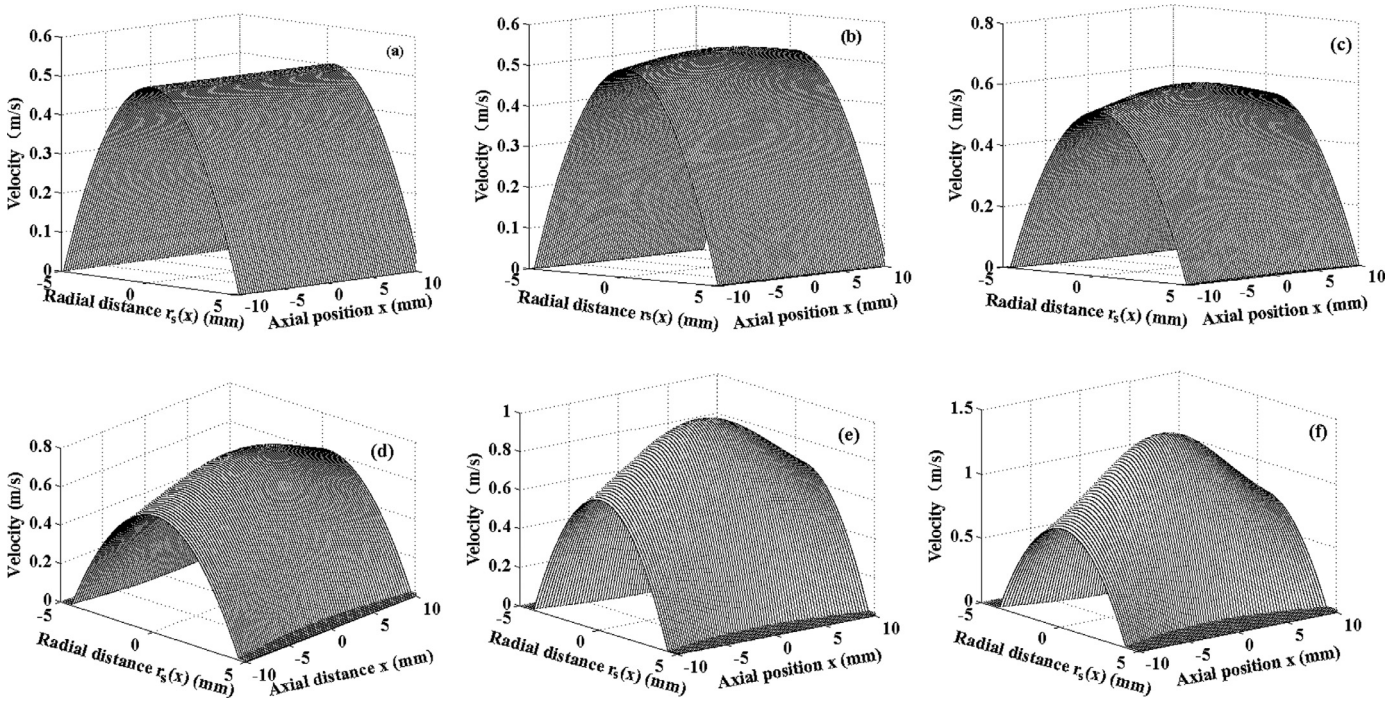

Fig. 3. Axial velocity distributions in vessels with different degrees of stenosis at time of systolic peak (0.2 s): (a) normal, (b) 5%, (c) 10%, (d) 20%, (e) 30%, and (f) 40%.

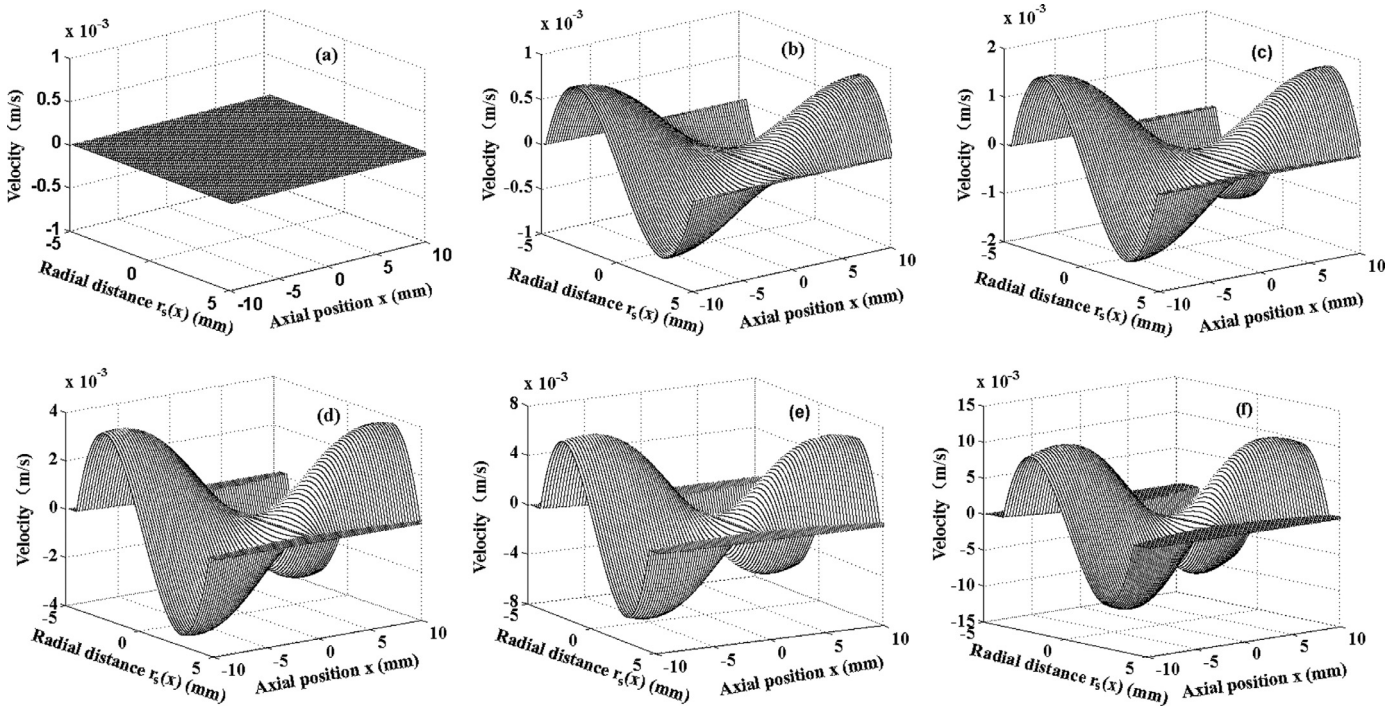

Fig. 4. Radial velocity distributions in vessels with different degrees of stenosis at time of systolic peak (0.2 s): (a) normal, (b) 5%, (c) 10%, (d) 20%, (e) 30%, and (f) 40%.

blood flow spectra by moving particles according to the constant velocity distribution at the narrowest position through a vessel with a constant radius of $R_0 - h$.

The vessel section is divided into K circular shells to calculate the blood flow power spectrum. When the division interval is small enough, it is reasonable to assume that all of the scatterers move with axial velocity v_k in the kth ($1 \le k \le K$) shell, and that the corresponding Doppler frequency is $f_k = \frac{v_k}{\lambda}\cos(\varphi)$, where λ is the wavelength. For a case with sample frequency f_s and observing time T_0, the total length of the signal sample is $M = T_0 \cdot f_s$. However, because of the various shell velocities v_k, the time durations ($tt_k = D/v_k$) for the particles passing through the insonated field D are different. The length of a Doppler signal with frequency f_k occupying the total length of sample signal $M$is

$$w_k = tt_k \cdot f_s = D/v_k \cdot f_s, \tag{11}$$

where $w_k \le M$. Thus, the spectrum produced by scatterer n is found as follows:

$$P_n(f_k, w_k, M) = \left(\frac{w_k}{M}\right)^2 \sin c^2\left[|f_k - n|\frac{w_k}{M}\pi\right], \tag{12}$$

where k represents the shell for the scatterer, and $1 \le n \le W$.

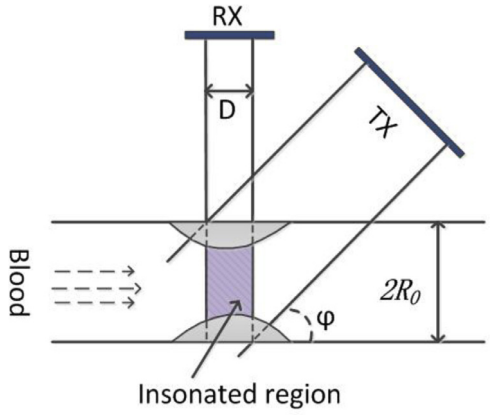

Fig. 5. Schematic of insonated vessel model. TX and RX represent transmitting and receiving transducers, respectively.

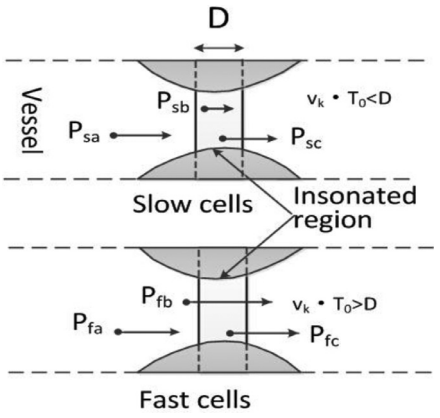

Fig. 6. Schematic diagram of fast cells (for instance, P_{fa}, P_{fb} and P_{fc}) and slow cells (for instance, P_{sa}, P_{sb} and P_{sc}). During observation time T_0, cells remain in (P_{sb}), or pass through (P_{fb}) the entire observational width D, while others do not (P_{sa}, P_{sc}, P_{fa} and P_{fc}).

In order to calculate the spectrum of total scatterers covered by the ultrasound field, the scatterers are divided into two groups (i.e., fast cells and slow cells) on the basis of whether or not the scatterers move beyond observation width D during the observation time T_0. If $v_k \cdot T_0 < D$, the scatters are defined as slow cells (shown at the top of Fig. 6); otherwise, they are defined as fast cells (shown at the bottom of Fig. 6). During observation time T_0, some slow cell remain in observational width D (for instance, P_{sb}), while others do not (for instance, P_{sa} and P_{sc}). During observation time T_0, some fast cells can pass through the entire observational width (for instance, P_{fb}), while others cannot (like P_{fa} and P_{fc}).

For the kth shell, the total number of scatterers passing through the insonated region during the observation time is calculated by multiplying density ρ_k by a corresponding volume. The density is defined as the number of scatterers per unit length in shell k; the volume is calculated by multiplying the scatterer moving distance and area of the circular shell in observation width D. Then, the spectrum of the total scatterers for the insonated vessel segment is obtained by accumulating the spectra of all the shells, each of which is calculated by multiplying the power of each scatterer described in Eq. (12) by the number of total scatterers in the shell. When the kth shell is for slow cells, the Doppler spectra of the scatterers passing through incompletely and remaining in the insonated region are respectively found using the following two equations:

$$SSa_k = \rho_k(D - v_k T_0)P(f_k, M, M) \tag{13}$$

$$SSb_k = \frac{2\rho_k v_k T_0}{M}\sum_{m=1}^{M-1} P(f_k, m, M), \tag{14}$$

where $\rho_k(D - v_k T_0)$ and $\frac{2\rho_k v_k T_0}{M}$, respectively, represent the cells passing through incompletely and the cells remaining in the insonated region. When the kth shell is for fast cells, the Doppler spectra of the scatterers passing through the insonated region incompletely and completely are respectively found as follows:

$$SFa_k = \rho_k D\left(\frac{T_0}{tt_k} - 1\right)P(f_k, w_k, M) \tag{15}$$

$$SFb_k = \frac{2\rho_k D}{w_k}\sum_{m=1}^{w_k-1} P(f_k, m, M), \tag{16}$$

where $\rho_k D(\frac{T_0}{tt_k} - 1)$ and $\frac{2\rho_k D}{w_k}$ are those passing through the insonated region incompletely and completely, respectively.

Finally, the total Doppler power spectrum is written as follows:

$$\begin{aligned} SP &= SSa_k + SSb_k + SFa_k + SFb_k \\ &= \sum_{k=1}^{k_D}\left[\rho_k(D - v_k T_0)P(f_k, M, M) + \frac{2\rho_k v_k T_0}{M}\sum_{n=1}^{M-1} P(f_k, m, M)\right] \\ &\quad + \sum_{k=k_D+1}^{K}\left[\rho_k D\left(\frac{T_0}{tt_k} - 1\right)P(f_k, w_k, M) + \frac{2\rho_k D}{w_k}\sum_{n=1}^{w_k-1} P(f_k, m, M)\right], \end{aligned} \tag{17}$$

where $k_D = D/(T_0 \cdot v_D)$ represents the transition shell between slow and fast shells. Readers are referred to the paper by Vilkomerson et al. [13] for a more detailed description of the spectrum model.

2.4. Determining frequency locations in spectra for maximum velocities

The Doppler spectra are calculated using Eqs. (11)–(17) based on the parameters listed in Table 1. The locations of the maximum frequencies are determined according to the intersections of the Doppler spectra and the theoretical maximum frequency shift f_{pd} obtained from the velocity distributions shown in Fig. 3. In Fig. 7, the dotted line represents the theoretical maximum Doppler frequency shifts, and the thick solid line represents the calculated spectra. From this figure, the theoretical maximum frequency shifts are found to increase along with an increase in the degree of stenosis, which is consistent with the variation in the maximum blood flow velocities in the vessels with different degrees of stenosis shown in Fig. 3. Compared with that of the normal vessel, the spectra for the stenotic vessels present different degrees of spectral broadening. These are shown by the spectral falling edges, which are very abrupt for normal vessels, but flat for stenotic ones. A higher degree of stenosis results in a more distinct spectral broadening, i.e., the falling edge will be more flat. This is because the Doppler signal echoed from a single scatterer is a windowed sine function, whose spectrum, as defined by Eq. (12), is the convolution of the spectral line and the spectrum of the rectangular window. The frequency of the spectral line corresponds to the scatterer moving velocity, and the spectrum of rectangular window can be expressed as a *Sinc* function during the observation time interval. Theoretically, the degree of broadening of the spectral line depends on the width of the window in the time domain. For a normal vessel, slow moving scatterers may spend a relatively long time or even the entire observation duration travelling in the insonated field. This will result in a relatively wide window with

Table 1
The parameters for the calculation of Doppler spectra.

Parameter	Value
Cardiac cycle T	1 s
The Doppler transmitting frequency f_0	8 MHz
The ultrasound velocity c	1540 m/s
The angle between the ultrasound beam and blood flow direction φ	45°
The observation width of vessel D	4 mm
The total length of vessel $4L$	80 mm
The length of wave λ	0.2 mm
The number of scatterers W	30,547 (resulting in a density of 10 scatterers/λ^3)
The number of circular shells K	40
The sample frequency f_s	30 kHz
The observation time T_0	10 ms
The total length of sample signal $M = T_0 \cdot f_s$	300

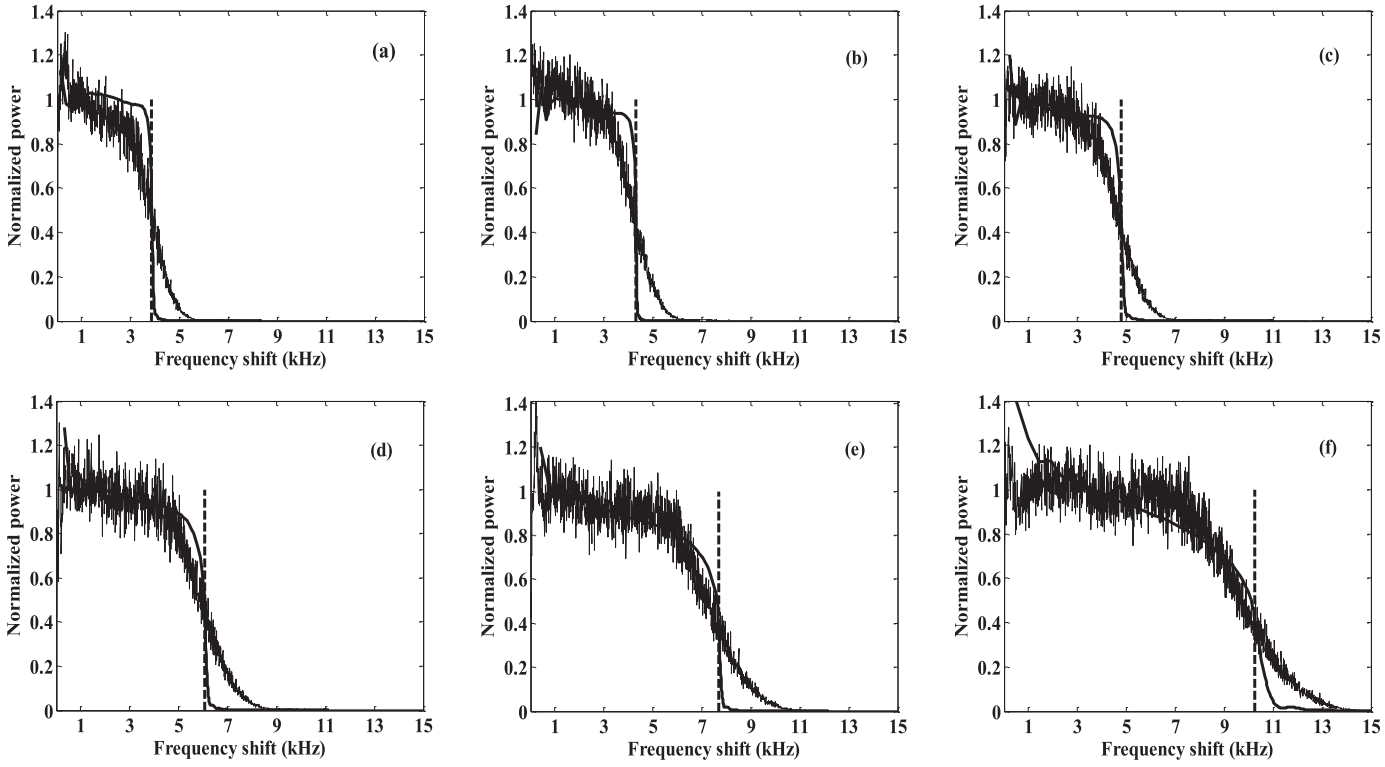

Fig. 7. Doppler blood flow spectral results of calculations and simulations for the vessel with different degrees of stenosis: (a) normal, (b) 5%, (c) 10%, (d) 20%, (e) 30%, and (f) 40%. The dotted line, thick solid line, and thin solid line denote the theoretical maximum Doppler frequency shifts, calculated spectra, and simulated spectra, respectively.

an effective signal in the time domain, as well as more spectral broadening in the frequency domain. However, for the narrowed vessels, the relatively high moving velocities of the blood flow result in more scatterers passing through the insonated region in less time. In this case, the effective signal is shortened during the observation time interval, which is equivalent to shortening effective width of the signals in the time domain, and widening the spectral line in the frequency domain. A higher degree of stenosis will result in faster movement of the scatterer, a shorter effective signal and greater spectral broadening. We also find from Fig. 7(a) that the location of the maximum frequency shift f_{pd} is the middle of the spectral falling edge in the normal vessel. This is in accordance with the result of Vilkomerson et al. who found a parabolic distribution of the blood flow velocity in a healthy artery [13]. However, Fig. 7(b)–(f) shows that the location of f_{pd} shifts downward, along with the Doppler spectral falling edge, with an increase in the stenosis. This is because the radial distributions of the axial blood flow velocities present sharper kurtosis in stenosed vessels, and the maximum velocities at the central axis of the vessel decrease more quickly in the radial direction. This leads to a reduction in the high-velocity component of the power spectra, especially for vessels with a higher degree of stenosis.

3. Simulation results and discussion

3.1. Locations of maximum frequencies in Doppler spectra

The simulation started with the generation of Doppler ultrasound blood flow signals from vessels modeled with different degrees of stenosis, as shown in Fig. 5 based on Field II. Field II [22] is an ultrasound simulation tool based on the linear acoustic theory. It is used for simulating the sound fields emitted and received by ultrasound transducers, as well as tissue scatterer distributions, from which the echoed radio frequency (RF) signals can be calculated. A model with a stepwise movement of the scatterers in an artery with a parabolic flow profile surrounded by tissue was used to simulate Doppler blood flow signals. It is demonstrated that the results could be used to study both spectral estimation techniques and color flow mapping estimators [23].

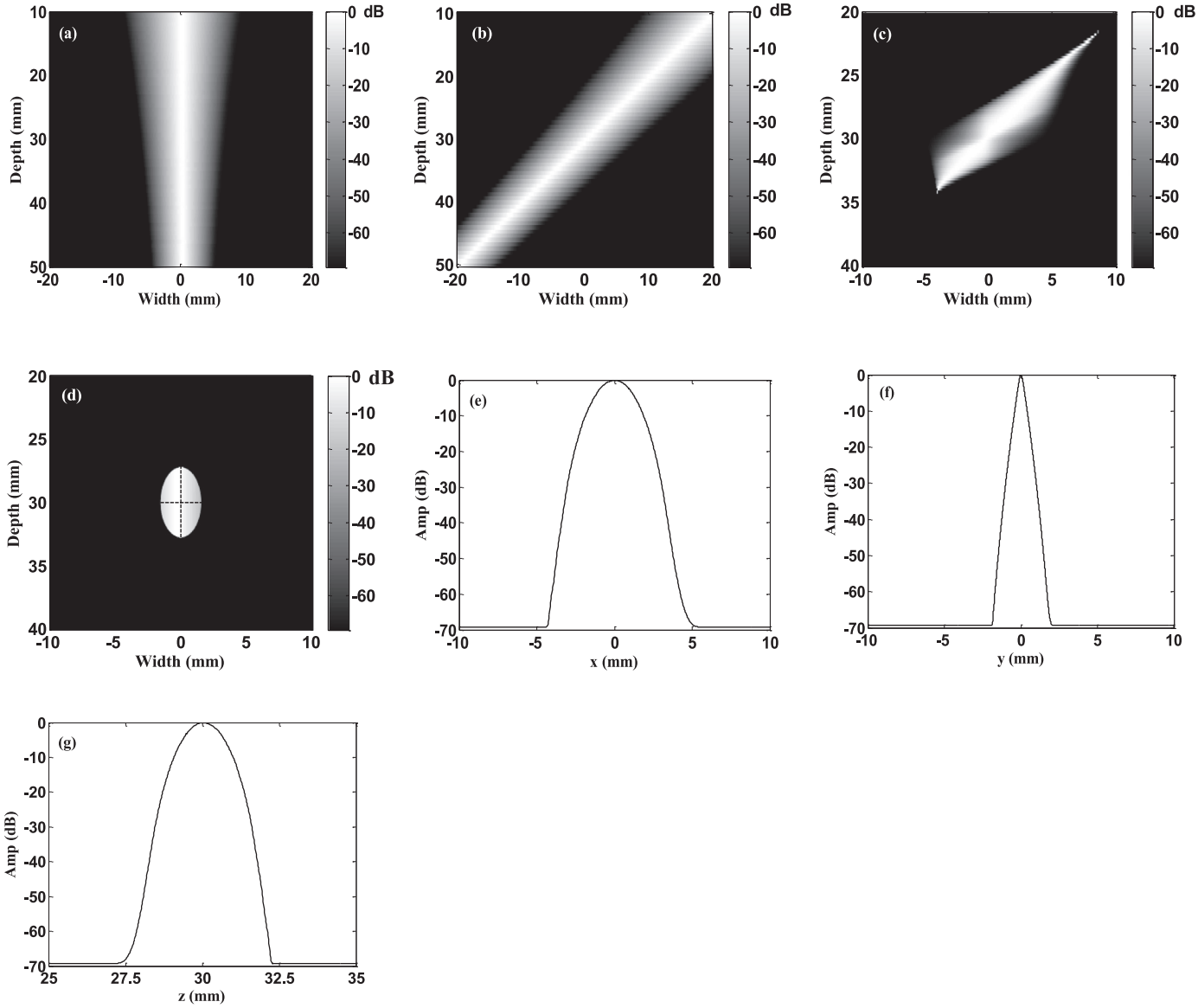

Fig. 8. Acoustic fields of transmission (a) and reception (b) from $x-z$ viewpoint at $y=0$ mm, as well as two-way versions from $x-z$ viewpoint at $y=0$ mm (c) and $y-z$ viewpoint at $x=0$ mm (d). The corresponding field profiles for the x ($y=0$ mm) and y ($x=0$ mm) axes at $z=30$ mm, and along the probe axis ($x=0$, $y=0$), are shown in (e), (f), and (g), respectively. They are simulated by Field II using flat round transducers with a radius of 10 mm.

In the simulation, the vessel model was placed at the central position of a rectangular scatterer phantom ($60\times20\times60$ mm), and flat round transducers were used. Each of them had a radius of 10 mm, and their panels were divided into basic 0.01×0.01 mm calculation elements, Fig. 8 shows the simulated acoustic transmission (a) and receiving (b) fields from the $x-z$ viewpoint at $y=0$ mm, as well as two-way versions from the $x-z$ viewpoint at $y=0$ mm (c) and the $y-z$ viewpoint at $x=0$ mm (d). The corresponding field profiles for the x ($y=0$ mm) and y ($x=0$ mm) axes at $z=30$ mm, and along the probe axis ($x=0$, $y=0$), are shown in (e), (f), and (g), respectively. The observed segment of the vessel is placed along the horizontal dashed line, whose point of intersection ($x=0$ mm, $y=0$ mm, and $z=30$ mm) with the vertical dashed line is the position of the center of the narrowest lumen. The insonation for the observed region of the vessel segment with a radius of 5-h mm and length of 4 mm is not uniform. Along the x (vessel axis) and y directions, the fields are almost constant inside the 6 dB extensions of 5.10 mm and 2.61 mm, respectively. However, there is a typical elliptical field with a 6 dB extension of 2.18 mm in the z direction. From the two-way fields shown in Fig. 8(c) and (d), it can be found that the acoustic pressure for the transmission and reception is focused at the position of $x=0$ mm, $y=0$ mm, and $z=30$ mm; the constant fields in the y and z directions are the narrowest.

The scatterers, which have an uniform position distribution and normal amplitude distribution in the phantom, are scanned repeatedly with sample frequency f_s. As described for the spectrum model (Section 2.3), the observed segment of the stenosed vessel could be approximately considered to be a tube with a constant radius of R_0-h, along which the scatterers move according to the axial velocity distribution at the narrowest position. During the scanning period, the echoed RF signals in each frame are obtained by moving the scatterers in the vessel, and then the Doppler ultrasound blood flow signals are obtained through the processes of quadrature demodulation, logarithmic compression and downsampling. Finally, the spectra for the entire insonated field are estimated using the STFT [24] from the accumulated Doppler blood flow signals in the radial direction. The spectra are

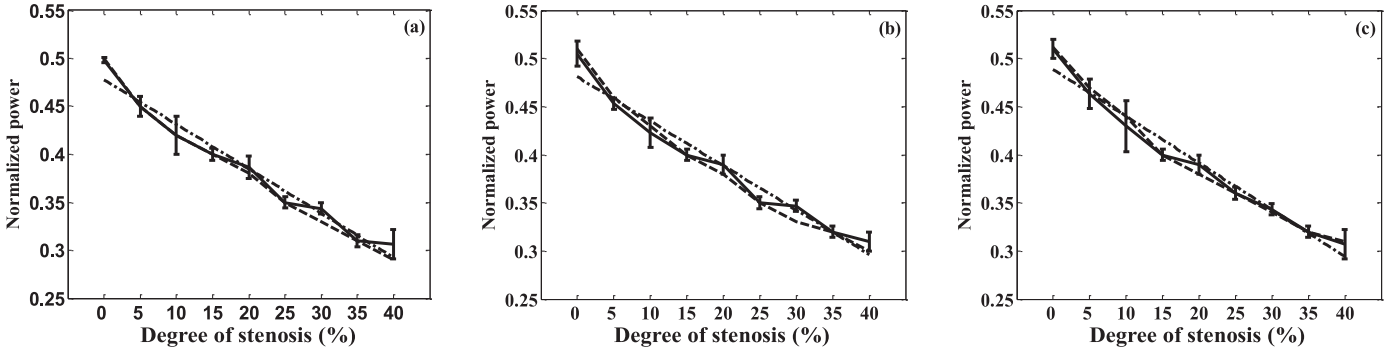

Fig. 9. Curves of percentile locations for f_{pd} along spectral falling edges plotted as functions of stenosis degree with different observed lengths: (a) 2 mm, (b) 4 mm, and (c) 6 mm. The dotted and solid lines represent the theoretical and simulated results (mean and standard deviation), respectively, and the dashed lines represent the linear fitting results from the mean values based on the simulation.

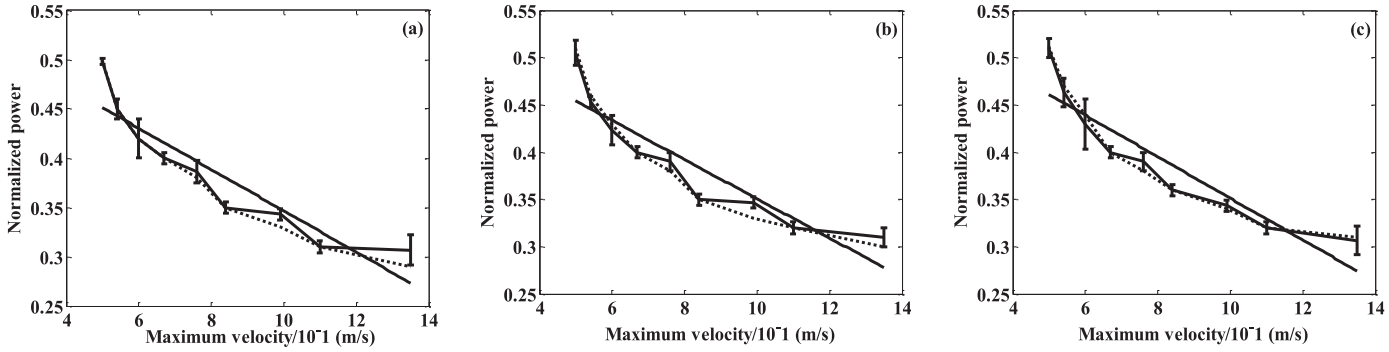

Fig. 10. Curves of percentile locations for f_{pd} along spectral falling edges plotted as functions of maximum velocity with different observed lengths: (a) 2 mm, (b) 4 mm, and (c) 6 mm. The dotted and solid lines represent the theoretical and simulated results (mean and standard deviation), respectively, and the dashed lines represent the linear fitting results from the mean values based on the simulation.

superimposed on Fig. 7 as thin solid lines. In general, the spectra obtained via the simulations are in accordance with those obtained from the theoretical calculations, except for random variations to a certain degree in the spectral curves obtained in the simulation. However, the Fourier spectra show some differences; for example, larger spectral broadening is observed in the simulation results, especially for the faster blood flow. Such discrepancies could be a result of the non-uniform insonation for the observed region of the vessel segment. From Fig. 8, the fields in the x (vessel axis), y, and z directions are only constant inside the 6 dB extensions of 5.10 mm, 2.61 mm, and 2.18 mm, respectively, which are narrower than the vessel radius, but wider than the length used in the calculation of the Doppler spectrum. The difference could also be due to the geometrical broadening caused by the acoustic field not being parallel to the blood flow direction in the simulation as a result of the circular transducers. A comparison of the maximum frequencyf_{pd} locations in the spectra based on the calculations and simulations, the coincident results validate the frequency location variation in the Doppler spectra for the maximum blood flow velocities in narrowed vessels.

3.2. Quantitative comparison and analysis

In order to quantitatively compare and analyze the variations in the maximum frequency locations in the Doppler blood flow spectra for the stenosed vessels, the observation widths of 4 mm, 8 mm, and 12 mm based on circular transducers with different radiuses of 1, 2, and 3 mm were tested, respectively. The curves of the power percentages for the f_{pd} locations along the spectral falling edges are plotted as the functions of the different degrees of stenosis (Fig. 9) or maximum blood flow velocities (Fig. 10) based on 20 sets of simulation data for comparison. The dotted and solid lines represent the theoretical and simulated results (mean and standard deviation), respectively, and the dashed lines represent the linear fitting results from the mean values based on the simulation.

From Fig. 9, it can be found that the theoretical calculation results are generally in good agreement with those of the simulations. However, because of the random variation in the amplitudes of the simulated Doppler blood flow signals, the relative standard deviations of the results obtained in the simulations vary from ±0.29% to ±2.0%, which are larger than the standard deviations of the results in the theoretical calculations (from ±0.01% to ±0.05%). For the normal vessel, f_{pd} is located at the middle of the spectral falling edge, i.e., the position of 0.51 normalized power, and this location shifts downward with an increase in the degree of stenosis. When the degree of stenosis increases to 40%, f_{pd} reaches the position of 0.32 normalized power with an approximately linear variation, which is verified by the linear fitting results,. Additionally, the results with the three different observation widths shown in Fig. 9(a)–(c) are in good agreement overall. This indicates that the variation in the radial direction of the axial velocities for different degrees of stenosis is the prime reason for the downward shift in the maximum frequency locations in the spectra along the spectral falling edges. On the other hand, the influence of the observation width (or the sample length of the signal in the time domain) is small.

Usually, in practice, the maximum velocities of the increased blood flow resulting from stenosis can be approximately measured using an ultrasound device [4]. Instead of the degrees of stenosis shown on the x axis in Fig. 9, Fig. 10 shows the curves of the percentile locations of f_{pd} in the spectral falling edges as functions of the maximum blood flow velocities. From Fig. 10, we find that the x axis represents blood flow velocities ranging from a minimum of 0.50 m/s for the normal vessel to a maximum of 1.38 m/s for

the vessel with 40% stenosis. Compared with the linear variations shown in Fig. 9, the percentile locations of f_{pd} shift downward nonlinearly with an increase in the maximum velocities. This is in agreement with the nonlinear relationship between the axial blood flow velocity distribution V_a and stenosis degree y described by Eq. (6).

However, the model used in the present study was based on a straight rigid tube with axially symmetric stenosis. These assumptions for blood vessels and stenosis are not satisfactory in practice. The modulation effects of a vessel wall with stenosis on the blood flow field were studied using a numerical model of pulsatile flow through a stenotic vessel with an amplitude oscillation [25]. Compared with that flowing through a rigid stenotic vessel, the flow velocity, and particularly the peak velocity, was increased in an elastic vessel [25]. This may result in the maximum frequency being located at a lower position on spectral falling edge compared to that for a rigid vessel. For plaques with other geometrical shapes, the results may also be affected because of the different axial velocity distributions. Based on the results for 42 patients who underwent an intra-vascular ultrasound (IVUS) procedure for a clinical indication of plaque morphology at the Cleveland Clinic Foundation, stenosis can be categorized into four types: peak-valley, ascending, descending, and diffuse [26]. In peak-valley stenosis, the axial velocity profile is symmetric throughout the stenosed portion of the artery, with an enhanced peak velocity occurring at the centerline. This type of stenosis could well be characterized by the geometrical model presented in this paper. However, according to numerical investigations of the effects of the other three types of plaque morphology on the flow characteristics, significant differences in the axial and radial velocity profiles of the velocity patterns are visible in both proximal and distal regions to the throat of maximum stenosis [27]. A stronger recirculation pattern close to the throat is found in descending stenosis, and it extends to a larger area compared to the other types. Thus, future research will be conducted on vessel models describing stenosis with other geometrical shapes, especially for descending stenosis, to find the maximum frequency locations in the spectra.

A clinical determination of the peak velocity from a Doppler spectrum is a routine operation to evaluate the blood blow conditions of vessels. It is also important to estimate the diagnosis parameters such as the S/D velocity ratio, RI, and PI for cardiac and cerebrovascular diseases [2,3]. Therefore, the accurate determination of the peak velocity in vessels is clinically significant, especially for those with different degrees of stenosis. It is hoped that the results presented in this paper can be employed to achieve accurate reproducible Doppler peak velocity measurements for axially symmetric stenosis in a clinical setting.

4. Conclusions

This paper presented an assessment of the variation in the Doppler frequency locations in the Doppler spectra for the maximum blood flow velocities in the vessels with different degrees of stenosis. The blood flow velocity distribution was determined using NSEs based on a geometric vessel model with bilaterial axisymmetric stenosis. Then, the Doppler spectra from an insonated segment of the vessel were calculated. The corresponding maximum frequency locations at the spectra were determined based on a comparison between the maximum blood flow velocities and calculated Doppler spectra. The simulation results were compared with the theoretical results for validation. It can be concluded from the theoretical and simulation results that the Doppler frequencies corresponding to the maximum velocities of blood flow for different degrees of stenosis were located at different positions on the spectral falling edge. The location was the middle of the falling edge for the normal vessel, and this location shifted downward along the falling edge with an increase in the degree of stenosis. When the stenosis reached 40%, the frequency location reached the position of 0.32 normalized power at the falling edge. The results may help improve the accuracy of a maximum blood flow velocity estimation from the Doppler blood flow spectra for axisymmetric stenosed vessels.

Ethical Approval

Not required.

Conflict of interest

None declared.

Acknowledgments

This work was supported by grants (61561049, 61561050) from the National Natural Science Foundation of China and the Key Project (2013FA008) from the Yunnan Provincial Natural Science Foundation.

References

[1] O'Leary DH, Polak JF, Kronmal RA, Kittner SJ, Bond MG, Wolfson SK Jr, et al.. Distribution and correlates of sonographically detected carotid artery disease in the Cardiovascular Health Study, 23. The CHS Collaborative Research Group; 1992. Stroke p. 1752–60.
[2] Sigel B. A brief history of Doppler ultrasound in the diagnosis of peripheral vascular disease. Ultras Med Biol 1998;24(2):169–76.
[3] Salonen R, Salonen JT. Progression of carotid atherosclerosis and its determinants: a population-based ultrasonography study. Atherosclerosis 1990;81(1):33–40.
[4] Evans DH, Evans DH, McDicken WN. Doppler ultrasound: physics, instrumentation, and signal processing. London: John Wiley & Sons Inc.; 2000. p. 179–83.
[5] Moraes R, Aydin N, Evans DH. The performance of three maximum frequency envelope detection algorithms for Doppler signals. J Vasc Invest 1995;1(3):126–34.
[6] Steinman AH, Tavakkoli J, Myers JG Jr, Cobbold RSC, Johnston KW. A new approach for determining maximum frequency in clinical Doppler ultrasound spectral estimates. In: Proceedings of the twenty-second annual international conference of the IEEE engineering in medicine and biology society, 2000, 4. IEEE; 2000. p. 2640–3.
[7] Östlund N, Yu J, Karlsson JS. Improved maximum frequency estimation with application to instantaneous mean frequency estimation of surface electromyography. IEEE Trans Biom Eng 2004;51(9):1541–6.
[8] Zhang Y. Method and apparatus for extracting an envelope curve of a spectrogram US Patent 7,611,467. 2009.
[9] Yu ACH, Steinman AH, Cobbold RSC. Transit-time broadening in pulsed Doppler ultrasound: a generalized amplitude modulation model. IEEE Trans Ultrason Ferroelectr Freq Control 2006;53(3):530–41.
[10] Pedersen MM, Pihl MJ, Haugaard P, Hansen JM, Hansen KL, Nielsen MB, Jensen JA. Comparison of real-time in vivo spectral and vector velocity estimation. Ultras Med Biol 2012;38(1):145–51.
[11] Übeylı ED, Güler I. Spectral analysis of internal carotid arterial Doppler signals using FFT, AR, MA, and ARMA methods. Comput Biol Med 2004;34(4):293–306.
[12] Zhang YF, Wang L, Gao YL, Chen JH, Shi XL. Noise reduction in Doppler ultrasound signals using an adaptive decomposition algorithm. Med Eng Phys 2007;29(6):699–707.
[13] Vilkomerson D, Ricci S, Tortoli P. Finding the peak velocity in a flow from its Doppler spectrum. IEEE Trans Ultrason Ferroelectr Freq Control 2013;60(10):2079–88.
[14] Galdi GP. An introduction to the mathematical theory of the Navier–Stokes equations: steady-state problems. Springer Science & Business Media; 2011.
[15] Liu ZR. Cardiovascular hydrodynamics, Shanghai: Fudan University Presses; 1986. (in Chinese).
[16] Finn R. On the exterior stationary problem for the Navier-Stokes equations, and associated perturbation problems. Arch Ration Mech Anal 1965;19(5):363–406.
[17] McLeod J. Computer simulation of the hydrodynamics of the cardiovascular system. Simulation 1964;2(3):33–41.
[18] Zarins CK, Giddens DP, Bharadvaj BK, Sottiurai VS, Mabon RF, Glagov S. Carotid bifurcation atherosclerosis: quantitative correlation of plaque localization with flow velocity profiles and wall shear stress. Circ Res 1983;53(4):502–14.
[19] Ku DN, Giddens DP, Zarins CK, Glagov S. Pulsatile flow and atherosclerosis in the human carotid bifurcation: positive correlation between plaque location and low oscillating shear stress. Arterioscler Thrombosis Vasc Biol 1985;5(3):293–302.
[20] Gao L, Zhang YF, Zhang KX, Cai GH, Zhang JH, Shi XL. A computer simulation model for Doppler ultrasound signals from pulsatile blood flow in stenosed vessels. Comput Biol Med 2012;42(9):906–14.

[21] Munk P, Jensen JA. A new approach for the estimation of the axial velocity using ultrasound. Ultrasonics 2000;37(10):661–5.
[22] Jensen JA, Svendsen NB. Calculation of pressure fields from arbitrarily shaped, apodized, and excited ultrasound transducers. IEEE Trans Ultrason Ferroelectr Freq Control 1992;39(2):262–7.
[23] Jensen JA, Munk P. Computer phantoms for simulating ultrasound B-mode and CFM images. Acoust Imag 1997;32:75–80.
[24] Brown JW, Churchill RV. Fourier series and boundary value problems, 10. AMC; 2012. p. 12.
[25] Zhang Q, Zhang Y, Zhou Y, Zhang K, Zhang K, Gao L. An ultrasound simulation model for the pulsatile blood flow modulated by the motion of stenosed vessel wall. BioMed Res Int 2016. doi:10.1155/2016/8502873.
[26] Beaumont R, Bhaganagar K, Segee B, Badak O. Using fuzzy logic for morphological classification of IVUS-based plaques in diseased coronary artery in the context of flow-dynamics. Soft Comput 2010;14(3):265.
[27] Bhaganagar K, Veeramachaneni C, Moreno C. Significance of plaque morphology in modifying flow characteristics in a diseased coronary artery: numerical simulation using plaque measurements from intravascular ultrasound imaging. Appl Math Model 2013;37(7):5381–93.